Science of the Total Environment 717 (2020) 137090

Contents lists available at ScienceDirect

Science of the Total Environment

journal homepage: www.elsevier.com/locate/scitotenv

Removal of thallium(I) from aqueous solutions using titanate nanomaterials: The performance and the influence of morphology

Nana Wang [a], Zebin Su [a], Nairui Deng [a], Yuyin Qiu [a], Liang Ma [b], Jianqiao Wang [a], Yuxiao Chen [a], Kaimei Hu [a], Chujie Huang [a], Tangfu Xiao [a,*]

[a] Key Laboratory for Water Quality and Conservation of the Pearl River Delta, Ministry of Education, School of Environmental Science and Engineering, Guangzhou University, Guangzhou 510006, China

[b] State Key Laboratory of Environmental Geochemistry, Institute of Geochemistry, Chinese Academy of Sciences, Guiyang 550081, China

HIGHLIGHTS

- Nanotubular and nanowire-like TNMs both own excellent Tl(I) adsorption ability.
- The morphology of TNMs has insignificant effect on Tl(I) adsorption behaviors.
- The order of inhibition effect on Tl (I) removal is Pb(II) > Cu(II) > Cd (II) > Zn(II).
- The α_M^{Tl} value of wire-like TNMs is up to 8.63, indicating a high Tl(I) selectivity.
- The adsorption mechanisms are similar but different in adsorption configurations.

GRAPHICAL ABSTRACT

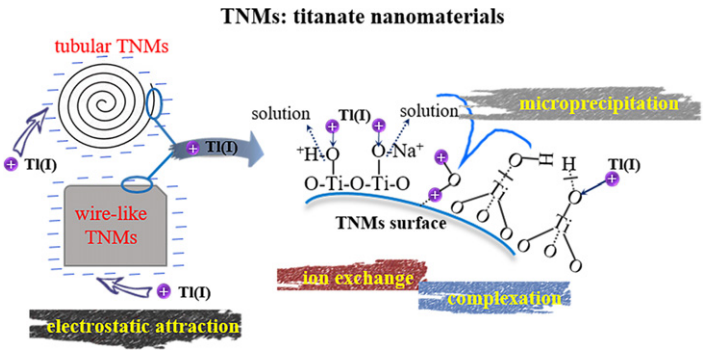

ARTICLE INFO

Article history:
Received 12 November 2019
Received in revised form 15 January 2020
Accepted 1 February 2020
Available online 3 February 2020

Editor: Xinbin Feng

Keywords:
Thallium
Titanate nanomaterials
Adsorption
Competition
Mechanism

ABSTRACT

Thallium (Tl) pollution has attracted environmental attention due to its high toxicity, thus the cleanup of Tl from the environment is of significance. Titanate nanomaterials (TNMs) with different morphologies can be synthesized via a hydrothermal reaction under different conditions but the knowledge of the Tl(I) removal by them is limited. Our results indicated that TNM prepared at 130 °C exhibited a nanotubular appearance and a longer reaction time resulted in the formation of perfect nanotube, while that prepared at 180 °C exhibited a nanowire-like arrangement. The nanotubular and nanowire-like TNMs possessed approximately excellent Tl (I) adsorption capacities, wide pH, and temperature application ranges but different adsorption kinetics. Inorganic ions influenced the Tl(I) removal and the inhibiting effect of heavy metal ions followed the sequence Pb (II) > Cu(II) > Cd(II) > Zn(II). The anti-interference ability and selectivity of wire-like TNMs for Tl(I) removal were higher than those of tubular TNMs. High Tl(I) uptakes of tubular and wire-like TNMs were driven by the electrostatic attraction, ion exchange with Na^+/H^+, and complexation with –ONa functional groups in the interlayers and Ti–OH on the surfaces of TNMs as well as microprecipitation; while their adsorption configurations were different. TNMs are promising for potential applications in Tl(I) elimination from wastewater due to the high adsorption capacity and regenerability. This work indicates that TNMs synthesized under different conditions have the similar Tl(I) adsorption performances and the preparation of TNMs used for Tl(I) removal has an undemanding synthesis condition.

* Corresponding author.
E-mail address: tfxiao@gzhu.edu.cn (T. Xiao)

https://doi.org/10.1016/j.scitotenv.2020.137090
0048-9697/

1. Introduction

Thallium (Tl), a toxic and non-essential trace metal to organisms, occurs widely in the natural environment, although it presents low concentrations in the natural hydrosphere and lithosphere (Xiao et al., 2003; Xiao et al., 2007; Tatsi et al., 2015; Belzile and Chen, 2017). The large release of Tl into the environment are primarily the result of industrial activities, including the emissions and solid waste from ferrous/nonferrous smelting operations, combustion of fossil fuels, and cement production (Xu et al., 2019). Toxicity studies have verified that Tl is highly toxic to humans and many other aquatic organisms, since Tl^+ has biogeochemical properties similar to K^+ and can be indiscriminately assimilated and bioaccumulated (Xiao et al., 2004; Madejón et al., 2007; Krasnodębska-Ostręga et al., 2012; Li et al., 2012). Tl can affect the respiratory, cardiovascular, gastrointestinal, peripheral, and central nervous systems; in addition, Tl exposure can lead to accidental, occupational or therapeutic poisoning or even death (Xiao et al., 2012; Rodríguez-Mercado and Altamirano-Lozano, 2013). Therefore, Tl has been added to the list of priority metallic pollutants by many governments (Jia et al., 2013). Although Tl is widely considered to be more acutely toxic than many other heavy metals, such as Hg, Cd and Pb (Twining et al., 2003; Law and Turner, 2011; Tatsi et al., 2015), and the awareness of the risk to human health and ecosystem safety resulted from Tl pollution is increasing, Tl has received only a small amount of attention. Currently, Tl contamination incidents are being successively reported and are an ongoing matter of concern, especially in China (Liu et al., 2019; Xu et al., 2019). Thus, there is an urgent need to establish safe Tl discharge standards and develop the Tl pollution control technology.

To minimize health risk arising from Tl, the stringent standards for Tl concentration have been established worldwide. For example, the United States Environmental Protection Agency (USEPA) has suggested the maximum permissible level at 2/140 μg/L in drinking water/industrial wastewater, while the more stringent limit of 0.1/5 μg/L was adopted in China (Liu et al., 2019; Xu et al., 2019). Tl mobilizes in an aquatic environment in the form of monovalent Tl(I) and trivalent Tl (III), while Tl(I) is usually the predominant specie in natural water and industrial wastewater due to the stronger thermodynamic stability (Sadowska et al., 2016; Jia et al., 2018). Thus, Tl(I) removal reaches a lower efficiency than other heavy metals because of the stronger mobility and lower permissible level. This poses a great technological hurdle for Tl(I) effective removal from solutions.

To date, various techniques, such as solvent extraction (Hassanien et al., 2017), ion exchange (Li et al., 2017a), oxidation/coagulation (Huangfu et al., 2017; Liu et al., 2017) and adsorption (Zhang et al., 2018) have been developed to remove Tl(I) from water/wastewater. Among these technologies, adsorption is considered as a leading treatment technique due to its high efficiency, low cost, convenient operation, and suitable for the removal of trace heavy metal (Carolin et al., 2017). So far, various adsorbents have been developed to remove Tl (I) from water/wastewater (Liu et al., 2019; Xu et al., 2019). It has been reported that titanate nanotube can exert higher adsorption ability for Tl(I) than many other adsorbents (Supplementary Material Table S1) because of the excellent characteristics such as large surface area to volume ratio, high chemical stability, strong interfacial reactivity, and cost-effectiveness (Sun and Li, 2003; Kanazawa et al., 2019; Simović et al., 2019; Liu et al., 2019; Xu et al., 2019). In addition, for titanate nanotube, there is no security risk produced from the dissolution of Ti^{4+} during the adsorption. This is a prominent advantage over other metal oxide, for example, manganese-based absorbents can produce Mn^{2+} owing to the oxidation reaction between Tl(I) and Mn(IV), which generates a new pollutant (Chen et al., 2017). Thus, titanate nanotube has a great application potential in the removal of toxic pollutants from water/wastewater. Previous studies have shown that titanate nanotube, prepared at 130 °C for 72 h after pre-stirring for 24 h, possess high efficiencies for the removal of Cd, Pb, Cr, Cu, U and Tl from solutions (Liu et al., 2013; Liu et al., 2014b; Liu et al., 2016).

However, the morphology and crystal phase of titanate nanomaterials (TNMs) synthesized by the hydrothermal treatment of TiO_2 and an alkali solution largely depended on the synthesis conditions (Wu et al., 2006). For example, Lee et al. (2008) reported that synthesis temperature induced a significant change in the phase structure of titanate compounds, and TNMs transformed from nanotube into nanorod with the higher synthesis temperature. Liu et al. (2014a) revealed that the morphology of the TNMs successively presented as nanogranules, nanoplates, nanotubes, nanosheets, and nanoblocks; moreover, the crystal phase changed from mixed to pure phase with increasing NaOH concentration. Li et al. (2015) observed that anatase was gradually transformed into titanate and TNMs changed from nanosheet to nanotube with increasing the hydrothermal reaction time. These studies also reported a higher removal efficiency of heavy metal for titanate nanotube rather than nanogranules, nanoplates, and nanosheets (Liu et al., 2014a; Li et al., 2015). Thus, the long-accepted and widely-used TNMs is titanate nanotube, synthesizing by heating TiO_2 and 10 M NaOH solution under 130 °C for 72 h after pre-stirring for 24 h, which is a bit time-consuming.

Currently, little information is available on Tl removal by tubular and wire-like TNMs. Liu et al. (2014b) just used titanate nanotubes, synthesized by the long-accepted method mentioned above, to achieve effective removal of Tl(I) and Tl(III), and reported that the adsorption mechanisms were ion-exchange and co-precipitation for Tl(III) while only ion-exchange for Tl(I). However, whether the changes of the morphology and crystallinity of TNMs prepared at different synthesis conditions can affect the Tl(I) adsorption performances, whether the Tl (I) adsorption behaviors of tubular and wire-like titanate are much different or similar, and whether the underlying mechanisms of Tl (I) removal change with the structural changes, these still remain unclear. A clear understanding of Tl(I) adsorption behaviors and mechanisms at molecular level is critical to assess the transport and fate of Tl (I) in treating wastewater. And the exploration about the differences of TNMs with different structures in Tl(I) removal efficiency serves to expand the application potential of TNMs.

Therefore, in this study, one wire-like and two tubular TNMs were prepared to remove Tl(I) from synthetic and natural water samples. Firstly, the characteristics of TNMs with different morphology and crystallinity were investigated and compared. Secondly, the Tl(I) adsorption properties of TNMs with different structures were compared to determine the effect of structure on the removal efficiency. Thirdly, the dominant mechanisms of TNMs with different morphology and crystallinity for Tl(I) removal were further explored and deduced. Lastly, the feasibility of regeneration and reuse and the treatment effects of natural waters were tested to evaluate the application of TNMs. The outcomes of this study will assist in understanding the effect of morphology of TNMs on Tl(I) removal and developing the feasible titanate nanomaterials for use in practical applications.

2. Experimental section

2.1. Materials

TiO_2, with a purity over 99%, was purchased from the Kermel Chemical Reagent Co., Ltd. (Tianjin, China) and used to synthesize TNMs without further purification. NaOH, $NaNO_3$, KNO_3, $Ca(NO_3)_2$, and HNO_3 were obtained from the Sinopharm Chemical Reagent Co., Ltd. (Shanghai, China). $TlNO_3$ (Sigma-Aldrich Co., USA), $Pb(NO_3)_2$, $Cd(NO_3)_2$, $Ni(NO_3)_2$, and $Zn(NO_3)_2$ (Adamas Reagent Co., Ltd., Basel, Switzerland) were used to investigate the competitive adsorption relationships between Tl(I) and heavy metal ions. All reagents were of analytical grade and directly used.

2.2. Synthesis of TNMs

The tubular and wire-like TNMs were synthesized via the alkaline hydrothermal method. To save time, we shortened the pre-stirring

time from 24 h to 2 h. Typically, 0.65 g of TiO_2 was first added to 65 mL of 10 M NaOH solution, after fully stirring for 2 h at room temperature, the reagent was transferred into a sealed Teflon autoclave (100 mL) and reacted at a certain temperature for several hours. When the reaction was finished and restored to room temperature, the precipitate was harvested and rinsed with ultrapure water until the washing solution pH was neutral. Then, the products were dried and ground for use. The nanomaterials prepared at 130 °C for 6 h, 130 °C for 72 h, and 180 °C for 30 h are referred to as TNM-6, TNM-72, and TNM-30, respectively. Herein, the TNM prepared at 180 °C for 30 h (TNM-30) was set as the control group, compared with the TNMs prepared at 130 °C (TNM-6 and TNM-72).

2.3. Analytical methods

Samples for solid-phase analysis were collected by centrifugation and dried when used for analysis. Changes in microstructure, morphology, elemental composition, crystal phase and chemical structure were examined by TEM (transmission electron microscopy), HRTEM (high resolution transmission electron microscopy), SEM-EDS (scanning electron microscopy-energy dispersive X-ray spectroscopy), XRD (X-ray diffraction), XPS (X-ray photoelectron spectroscopy), FTIR (Fourier transform infrared spectroscopy), and BET (the N_2 Brunauer-Emmett-Teller theory). The detail analytical methods are shown in the Supplementary Material.

All solution samples after reaction were filtered through 0.45 μm polyether sulfone (PES) filter membranes for the determinations of Tl (I) and other metal ions. The concentrations of heavy metals were analyzed by an atomic absorption spectrometer (AAS, 900T, PerkinElmer Co., USA) equipped with the corresponding metal hollow-cathode lamps and air-acetylene flame.

2.4. Adsorption experiments

All batch experiments were conducted in 50 mL conical tubes with 20 mL of solution and 5 mg of TNMs, shaking in a thermostatic shaker at 180 rpm and 25 °C for 12 h (unless otherwise specified). In order to obtain the exact adsorption ability—impact factor curves, laboratory adsorption studies usually use a considerably higher adsorbate concentration than that expected in natural aqueous media. Thus, the experiments in this study were conducted with a concentration of several hundred milligrams per liter. And the experiments were performed at the optimal pH value, at which point the removal efficiency was more excellent, but apart from the batch experiment of the effect of solution pH. Each experiment was conducted in triplicate, and the average values were calculated with the standard deviations, which are indicated as error bars in the graphs below. The adsorption capacities of TNM-6, TNM-72, and TNM-30 for Tl(I) were compared under the same conditions. The Tl(I) adsorption capacity q_e (mg/g) and removal efficiency R (%) were calculated according to Eqs. (1) and (2), respectively:

$$q_e = \frac{(c_0 - c_e)V}{m} \tag{1}$$

$$R = \frac{c_0 - c_e}{c_0} \times 100\% \tag{2}$$

where c_0 and c_e are the initial and equilibrium concentrations of Tl(I), respectively; V (mL) is the volume, and m (g) is the mass of TNM. The specific experimental conditions are described in the following sections.

2.4.1. Adsorption kinetics

The adsorption kinetics of Tl(I) on TNM-6, TNM-72, and TNM-30 were examined with a 200 mg/L Tl(I) solution (pH = 8.0 ± 0.2) and 0.25 g/L adsorbent. The samples were taken at specific time intervals, with a maximum interval of 24 h to research the perfect adsorption equilibrium. The experimental data were fitted with the pseudo-first order (PFO), pseudo-second order (PSO) and intraparticle diffusion models given below (Wang et al., 2016; Yin et al., 2017):

$$\ln(q_e - q_t) = \ln(q_e) - k_1 t \tag{3}$$

$$\frac{t}{q_t} = \frac{1}{k_2 q_e^2} + \frac{1}{q_e} t \tag{4}$$

$$q_t = k_{id} t^{0.5} + C_{id} \tag{5}$$

where q_t (mg/g) is the adsorption capacity of TNMs at any time t (h), k_1 (1/h) and k_2 (g/mg·h) are the PFO and PSO rate constants, respectively; k_{id} (mg/g·h) is the intraparticle diffusion rate constant and C_{id} (mg/g) is the intercept at different diffusion stages, representing the boundary layer effect.

2.4.2. Adsorption isotherms

To determine the maximal Tl(I) adsorption capacities of TNM-6, TNM-72, and TNM-30, batch tests were performed with various initial Tl(I) concentrations ranging from 25 to 600 mg/L at 25, 35, and 45 °C (pH = 8.0 ± 0.2) for 12 h. To explain the experimental data, the Langmuir adsorption model (Eq. (6)), Freundlich model (Eq. (7)), and Temkin model (Eq. (8)) were employed (Wang et al., 2016; Zhang et al., 2018).

$$\frac{c_e}{q_e} = \frac{1}{K_L q_m} + \frac{c_e}{q_m} \tag{6}$$

$$\log q_e = \log K_F + \frac{1}{n} \log c_e \tag{7}$$

$$q_e = \frac{RT}{b} \ln a + \frac{RT}{b} \ln c_e \tag{8}$$

where q_m (mg/g) is the maximum adsorption capacity, K_L (L/mg) and K_F (mg/g) are the Langmuir and Freundlich coefficients, respectively; n represents a heterogeneity factor (a lower value indicates a more homogeneous surface), b (kJ/mol) is the Temkin constant related to the adsorption heat and a (L/mg) is the Temkin isotherm constant.

2.4.3. Effects of the solution pH and coexisting ions

The pH value of Tl(I) solution (200 mg/L) was adjusted with dilute HNO_3 and/or NaOH solution to a target pH value between 2.0 and 11.0. The corresponding equilibrium pH was measured after adsorption. Metal cations such as K(I), Na(I), and Ca(II) largely exist in natural waters and industrial wastewaters. The coexistence of these ions might interfere with the removal of target metal ion. Thus, the effects of these coexisting ions on the Tl(I) adsorption of TNMs were examined by adding a determined amount of $NaNO_3$, KNO_3, and $Ca(NO_3)_2$ into a 200 mg/L Tl(I) solution, to maintain an ion concentration in the range of 0.01 to 2.0 M. The corresponding pH was fixed at the optimal pH value determined by the result of solution pH batch experiment, largely close to the value of natural water.

2.4.4. Competitive adsorption of Tl(I), Pb(II), Cu(II), Cd(II), and Zn(II)

In addition, heavy metal cations such as Pb(II), Cu(II), Cd(II), and Zn (II) coexist commonly with Tl(I) in industrial effluents. The understanding of the competition for the active sites of TNMs with Tl(I) and the adsorption selectivity of TNMs to Tl(I) is important for evaluating the application feasibility of TNMs in the wastewater treatment. Therefore, two competitive adsorption experiments were performed: 1) competitive adsorption in a binary system experiments were conducted by mixing Tl(I) with another heavy metal ion, e.g. Tl/Pb, Tl/Cu, Tl/Cd, and Tl/Zn. Herein, the concentration of Tl(I) was fixed at 200 mg/L, and the concentrations for the other heavy metal ions varied from 5 to

100 mg/L; 2) a quinary adsorption system was obtained by mixing five heavy metal ions (Tl/Pb/Cu/Cd/Zn system) with identical initial concentrations varied from 1 to 100 mg/L.

To further evaluate the adsorption preference of TNMs in the presence of two different heavy metal ions in the binary system, the separation factor α_M^{Tl} was calculated and analyzed:

$$\alpha_M^{Tl} = \frac{q_{e,Tl} c_{e,M}}{q_{e,M} c_{e,Tl}} \quad (9)$$

where $q_{e,Tl}$ and $q_{e,M}$ (mg/g) are the adsorption capacities of Tl(I) and another heavy metal ion at equilibrium, respectively; $c_{e,Tl}$ and $c_{e,M}$ (mg/L) are their corresponding equilibrium concentrations.

2.5. Efficient removal of Tl(I) from spiked Pearl River water

The water samples were collected from the Pearl River in South China, according to the national standard sampling method, and then the determined exogenous thallium nitrate was added to obtain Tl (I) concentrations of 141.5, 5512.3, and 27,384.1 μg/L, eventually used to investigate the ability of TNMs to effectively remove trace and macro levels of Tl(I) from natural wastewater. Herein, 5 mg of TNM-6, TNM-72, and TNM-30 were added into 20 mL of the abovementioned Tl(I) solutions and shaken at 180 rpm for 12 h at room temperature. The residual concentrations of Tl(I) and other metal(loid) ions in the supernatants were measured using inductively coupled plasma-mass spectrometry (ICP-MS, NexION 300×, PerkinElmer Inc., USA).

3. Results and discussion

3.1. Characteristics of the three TNMs

Elemental analyses indicated that the prepared TNM-6, TNM-72, and TNM-30 all have the same elementary composition, including O, Ti, and Na, whereas the marked differences in morphology were observed among these three TNMs (Fig. 1 and Fig. S1). TNM-6 and TNM-72 prepared at 130 °C both appear as anfractuous nanotubes aggregated in clusters, which contributes to the settlement of nanostructured titanate material; whereas TNM-30 prepared at 180 °C exhibits a wire-like scattered arrangement (Fig. S1), then it owns a better dispersion than nanotubular TNMs in the solution, which was accordance with the experimental phenomena. As seen in the TEM and HRTEM images (Fig. 1), TNM-6 prepared with 6 h is characterized by uniformly hollow and open-ended tubes with a small inner diameter of 3.8 nm and outer diameter of 8.8 nm, while the boundary between the layers of the tubes was not clear and the lamellar structures were also observed on the surface of the tubes. A longer reaction time (72 h) makes the nanotubes more perfect with an inner diameter of 4.8 nm and outer diameter of 9.8 nm, which were larger than those of TNM-6. These nanotubes presented a distinct multiwalled tubular structure with an interlayer distance of 0.6 nm, but the multiwalled structure was asymmetric, i.e., it contained five layers on one side and three layers on the other side. This finding indicated that the tubes were formed by scrolling conjoined multilayer nanosheets (Wu et al., 2006). However, TNM-30 (Fig. 1c) presents a scattered arrangement of filled nanowires with an inhomogeneous size distribution for both the length and width; and the two sets of lattice fringes of these well-crystallized nanowires were resolved with spacings of 1.5 nm and 0.6 nm. At higher temperatures, the thickness of the lamellar structures quickly increased, and then these thick layers split between the (100) planes of $Na_2Ti_nO_{2n+1}$ to form nanowires instead of nanotubes. To decrease the free energy, the thin lamellar structures also condensed themselves by folding to form thick wires, accompanying with the sharp decrease in the titanate interlayer spacing, specific surface area, and pore volume (Wu et al., 2006). The BET specific surface areas of TNM-6, TNM-72, and TNM-30 were 174.85, 203.37, and 38.52 m^2/g with corresponding pore volumes of 0.87, 1.13, and 0.24 cm^3/g, respectively. It appears that the obvious differences in surface area and pore volume of the three TNMs are related to their morphology which itself is dependent on the synthesis conditions.

According to the XRD patterns (Fig. 2a), TNM-6, TNM-72, and TNM-30 are characterized by the intense characteristic peaks at approximately 10°, 24°, 28°, and 48°, which are assigned to the (001), (002), (003) and (020) facets of $Na_2Ti_3O_7$, indicating a successful synthesis with the structure of titanate (Thorne et al., 2005; Liu et al., 2013; Liu et al., 2014a; Liu et al., 2014b; Yin et al., 2017). The nanowire-like TNM shows well resolved peaks compared to nanotubular TNMs. There was less obvious crystalline rutile and anatase phases in TNM-72 than in TNM-6 and TNM-30. The characteristic peak at approximately 10° was stronger for TNM-30 than for TNM-6 and TNM-72, indicating the larger proportion of the interlayer spacing of titanate. This means the higher exchange potential of Tl(I) with Na^+/H^+. The diffraction peaks at approximately 24° and 28° were more intense for TNM-6 and TNM-72 than for TNM-30, which implied a larger proportion of sodium titanate nanotubes in TNM-6 and TNM-72. The typical synthetic process including hydrothermal and washing processes can be expressed as follows (Thorne et al., 2005; Liu et al., 2014a): $2NaOH + nTiO_2 + xH_2O \rightarrow Na_2Ti_nO_{2n+1}\cdot xH_2O + xH_2O \rightarrow (Na, H)_2Ti_nO_{2n+1}\cdot xH_2O + xNaOH$. Herein, the corrugated ribbons of edge-sharing [TiO_6] octahedrons and Na^+/H^+ situated in the interlayers were composed of the universal structure of $(Na, H)_2Ti_nO_{2n+1}$.

The FTIR spectra of all three TNMs also confirmed that they owned similar typical adsorption bands (Fig. 2b), including the broad intense peaks at 3430 and 1634 cm^{-1} ascribed to the characteristic vibration of O-H and the stretching vibration of Ti-OH band, the band around 905 cm^{-1} characterized by the stretching vibration of non-bridging oxygen atoms ($TiO(ONa)_2$), which was strongly affected by the interlayer ions, and the wide peak at 475 cm^{-1} attributed to the Ti-O vibration in [Ti-O_6] octahedra (Yin et al., 2017). However, wire-like TNM-30 had more active –OH based on the blunt peak at approximately 3200 cm^{-1}, whereas tubular TNM-6 had fewer $TiO(ONa)_2$ groups, as indicated by the incomplete peak at approximately 905 cm^{-1}. Therefore, the types of adsorption site on the three TNMs synthesized under different conditions are approximately same, but these TNMs owned different morphologies. This is attributed to the differences in the contents of functional groups and the arrangement of lamellar structures caused by the change of surface energy (Wu et al., 2006).

3.2. Tl(I) adsorption

3.2.1. Adsorption kinetics of Tl(I) by TNMs

As shown in Fig. 3a, the Tl(I) adsorption capacity remarkably increased within the first 15 min for TNM-6 and TNM-72, while the same phenomenon was observed within 2 h for TNM-30. In longer trials, i.e., up to 2 and 12 h, all adsorption reactions slowly reached equilibrium. Although the nanotubular structure of TNM-6 was imperfect, compared with that of TNM-72, there was no obvious difference in the adsorption equilibrium time. However, the nanowire-like TNM-30 had a significantly longer equilibrium time than the nanotubular TNMs. This difference might be due to their different structures. The larger specific surface areas and pore volumes were endowed to the tubular TNMs rather than the wire-like TNM-30, which could provide more opportunities for Tl(I) to contact with the binding sites.

Model parameters for the adsorption kinetics are presented in Fig. S2 and Table S1. The PSO model demonstrates an excellent fit to the experimental data compared to the PFO model, as indicated by the higher correlation coefficients ($R^2 = 1$). This result indicated that chemical adsorption played an important role in the Tl(I) uptake process. The low K_2 values imply the high affinity of Tl(I) for the adsorbent active sites and the fast uptake process of Tl(I) on TNMs. The Tl(I) initial adsorption rate v_0 ($v_0 = K_2 q_e^2$) on TNMs was in the order of TNM-6 > TNM-72 > TNM-30. These results combined with the adsorption

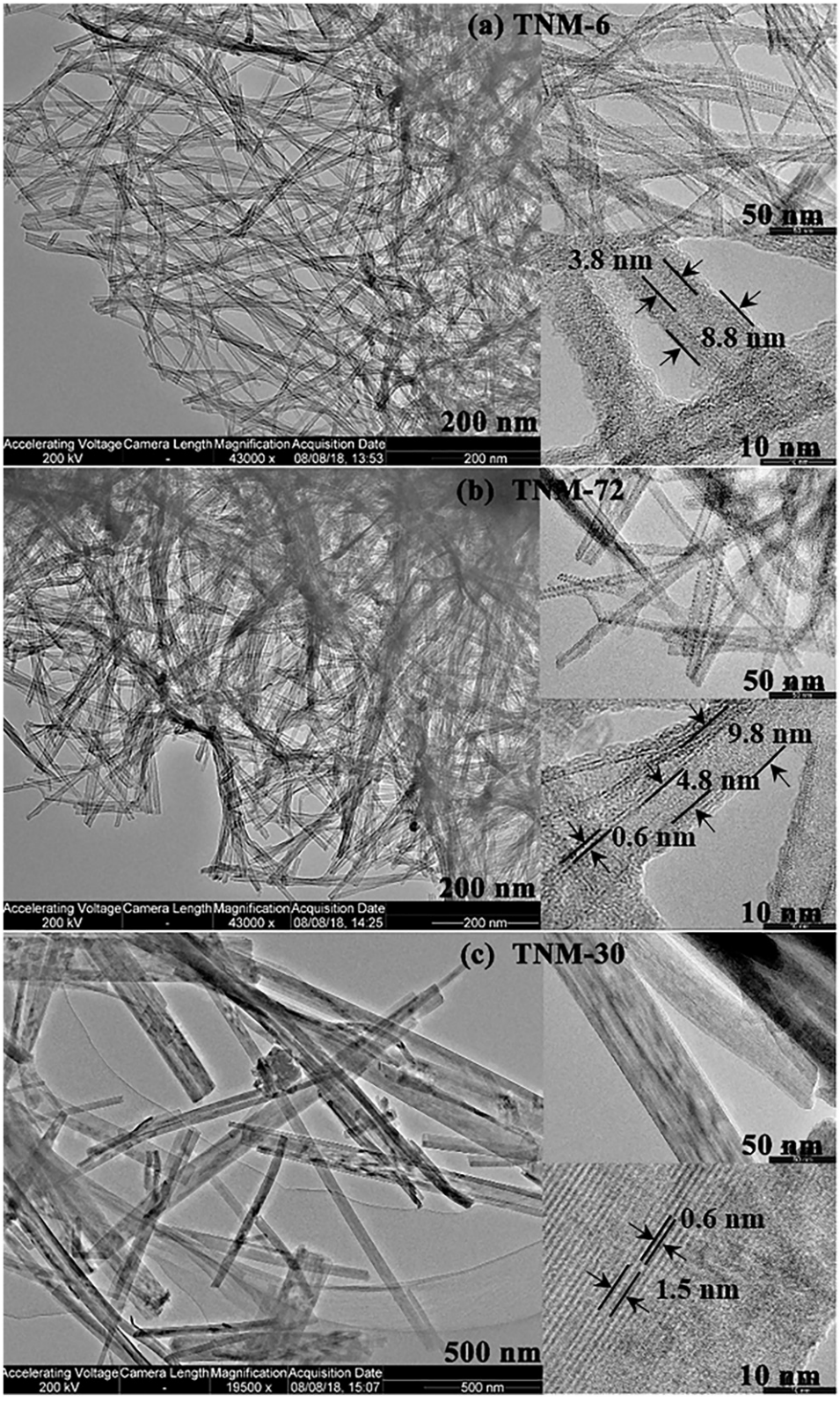

Fig. 1. TEM and HRTEM images of (a) TNM-6, (b) TNM-72 and (c) TNM-30.

equilibrium time results showed that TNM-6 has a time advantage, which is of significant practical importance.

The PSO model successfully revealed the driving force of the adsorption reaction but failed to describe the whole adsorption process; thus, the intraparticle diffusion model was also employed to fit the experimental data. The plots (q_t versus $t^{0.5}$) of Tl(I) adsorption on TNM-6, TNM-72, and TNM-30 (Fig. S2c) all presented multilinear correlations, i.e., three stages occurred during the adsorption process: fast external surface adsorption (film diffusion), intraparticle diffusion, and absorption equilibrium. The $k_{id,i}$ values shown in Table S1 remarkably decreased from $k_{id,1}$ to $k_{id,3}$ while the C_{id} values exhibited an opposite trend, indicating that both film and intraparticle diffusion played

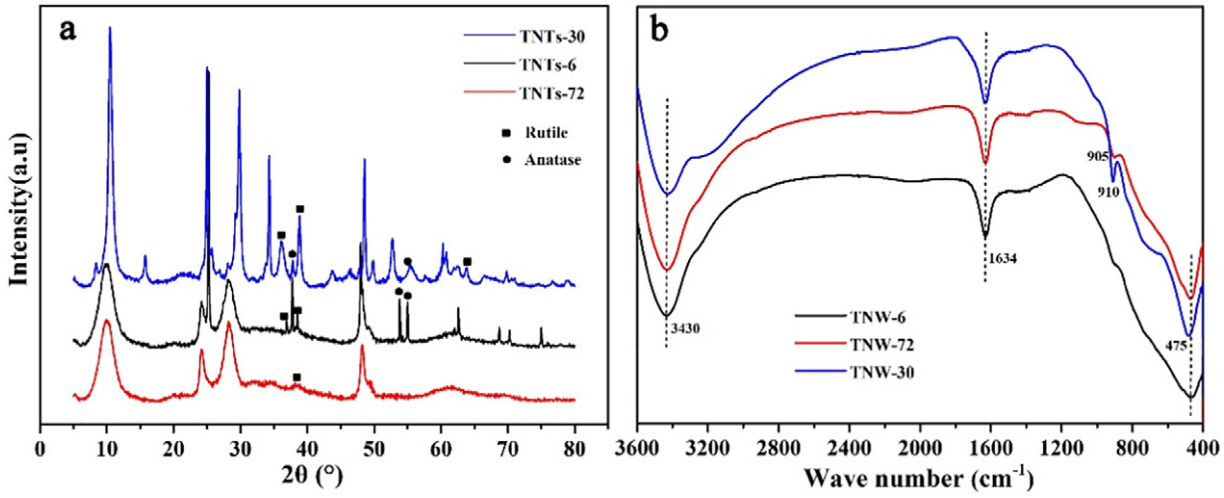

Fig. 2. XRD (a) and FTIR (b) patterns of TNM-6, TNM-72, and TNM-30.

important roles in the Tl(I) adsorption process. The tubular TNMs has a higher boundary layer effect than the wire-like TNM.

3.2.2. Adsorption isotherms of Tl(I) by TNMs

Fig. 3b shows the effect of the initial Tl(I) concentration on the Tl (I) adsorption capacity of TNMs at 25, 35, and 45 °C. The Tl(I) adsorption capacities of TNMs at different temperatures significantly increased at low initial concentrations, then slowly increased and finally remained constant in the high concentration range. These results indicated the effectiveness of the as-prepared TNMs for Tl(I) removal.

The Langmuir, Freundlich, and Temkin models were employed to reveal the interaction between Tl(I) and TNMs (Fig. S3). According to the correlation coefficient R^2 values (Table S2), the Langmuir isotherm ($R^2 = 1$) better described the TNMs adsorption behaviors than the Freundlich and Temkin models, indicating a monolayer chemical adsorption site and homogeneous adsorption energy. This result was further proven by the values of b_T, i.e., approximately and/or over 40 kJ/mol, which are in the bonding energy range of chemisorption. The n values were >1, implying a feasible adsorption process with favorable binding adsorption. The maximum adsorption capacities of Tl(I) on TNM-6, TNM-72, and TNM-30 were 609.756, 657.895, and 710.400 mg/g, respectively, which were identical to the experimental results. The gap of Tl(I) adsorption ability of TNM-6/TNM-72 and TNM-72/TNM-30 was equal and only close to 50 mg/g. This indicated that the Tl(I) removal efficiency was insignificantly dependent on the morphology and crystal structure of TNMs.

The thermodynamic calculation (Table S4) indicated that the adsorption capacity of Tl(I) slightly increased with increasing temperature. The negative values of △G implied that the Tl(I) adsorption on the three TNMs was naturally spontaneous. The positive △H values indicated that the adsorption process was endothermic, since the complexation of Tl(I) with the surface sites of TNMs was a dehydration process. The structural disorder at the solid/water interfaces after Tl (I) adsorption was enhanced according to the positive △S values. The △H and △S values of nanowire-like TNMs were higher than those of nanotubular TNMs, indicating a larger inherent energetic change during the Tl(I) adsorption process. Thus, Tl(I) adsorption capacity of nanowire-like TNMs was slightly higher than those of nanotubular TNMs.

3.2.3. Effects of the solution pH and coexisting ions

The effect of pH on Tl(I) adsorption by TNMs was examined in the range of 2 to 11. Herein, no buffer solutions or other efforts were used to maintain the solution pH. Fig. S4a indicated that Tl(I) adsorption on TNM-6, TNM-72, and TNM-30 had the same tendency with pH increase and owned a broad pH application range. The pH_{pzc} values of TNM-6, TNM-72, and TNM-30 were between 3 and 4 (Fig. S4b). Tl^+ is the predominant species of monovalent thallium in a wide pH range. Therefore,

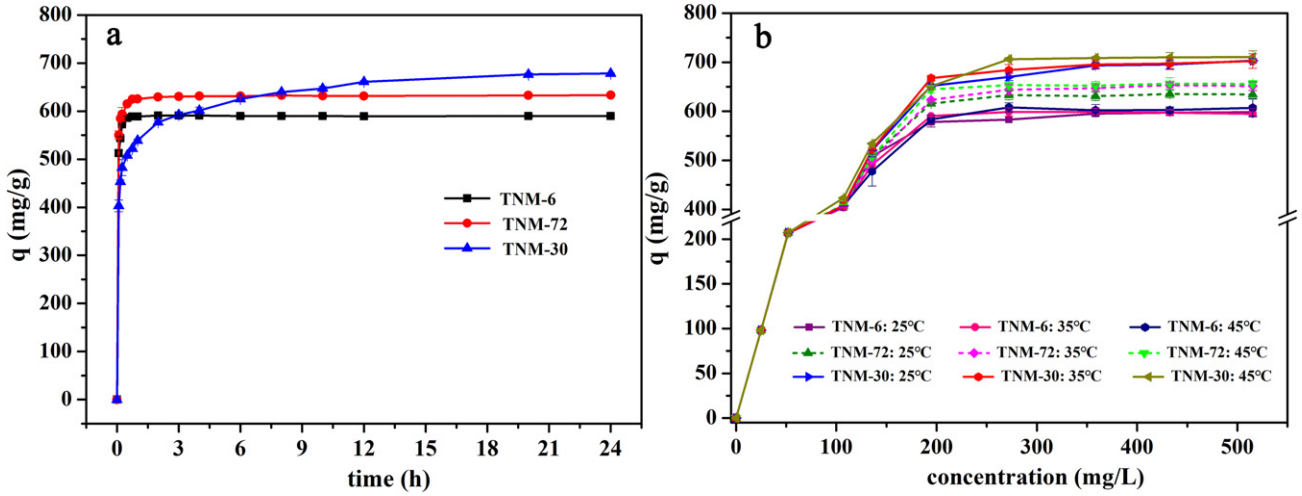

Fig. 3. Effects of (a) adsorption time and (b) initial concentration on Tl(I) adsorption by TNM-6, TNM-72, and TNM-30 (pH 8.0, adsorbent dosage 0.25 g/L).

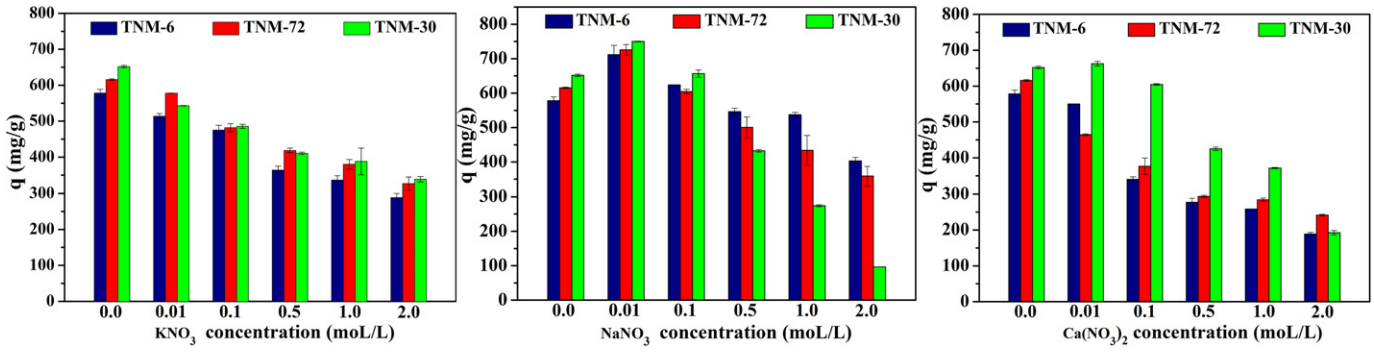

Fig. 4. Effects of coexisting K^+, Na^+, and Ca^{2+} ions on Tl(I) adsorption by TNM-6, TNM-72, and TNM-30 (pH 8.0, adsorbent dosage 0.25 g/L, Tl(I) concentration 200 mg/L, 25 °C).

the lower Tl(I) adsorption ability occurred at pH < 4, due to the competitive effect of excess H^+ and Tl^+ and the electrostatic repulsion between the positively-charged TNMs and Tl^+ caused by the favorable protonation reaction. When the pH increased over 4, TNMs became negatively-charged and the coexisting H^+ ions in solution dramatically dropped, corresponding to a continuous increase in Tl(I) adsorption capacity. Moreover, the final pH increased within the initial pH range of 3–6 and decreased when the initial pH exceeded 7. Considering the increase in the Na^+ concentration in solution after adsorption (data not shown), the above phenomenon was attributed to a preferential Na^+ exchange and a subsequent H^+ exchange. H^+ participated in the protonation of hydroxyl groups on TNMs under acid conditions, while an ion exchange reaction with Tl^+ occurred under alkaline conditions.

Given the effects of coexisting K^+, Na^+, and Ca^{2+} ions, the Tl (I) adsorption capacity of the three TNMs decreased with increasing concentrations of metal ions as a whole (Fig. 4). The effect of K^+ on Tl (I) adsorption by the tubular and wire-like TNMs was similar. This was because that (i) K^+ and Tl^+ ions possess similar ionic radii and chemical properties, and (ii) the tubular and wire-like TNMs owned similar adsorption sites, then K^+ identically interfered with the reaction between Tl(I) and binding sites on the surface of tubular and wire-like TNMs. For Na^+, Tl(I) removal was promoted at a low Na^+ concentration while slightly inhibited at the higher concentration. During the Tl (I) adsorption process, monovalent Na^+ largely existed in the interlayer spacing of titanate served as the ion exchange sites. The wire-like TNMs owned a larger proportion of the interlayer spacing than tubular TNMs, therefore, the ability of TNMs to resist Na^+ interference followed titanate nanotubes > titanate nanowires. However, the ability to resist Ca^{2+} interference exhibited an opposite order. This was due to the affinity of bivalent Ca^{2+} to TNMs, based on the different valence states and

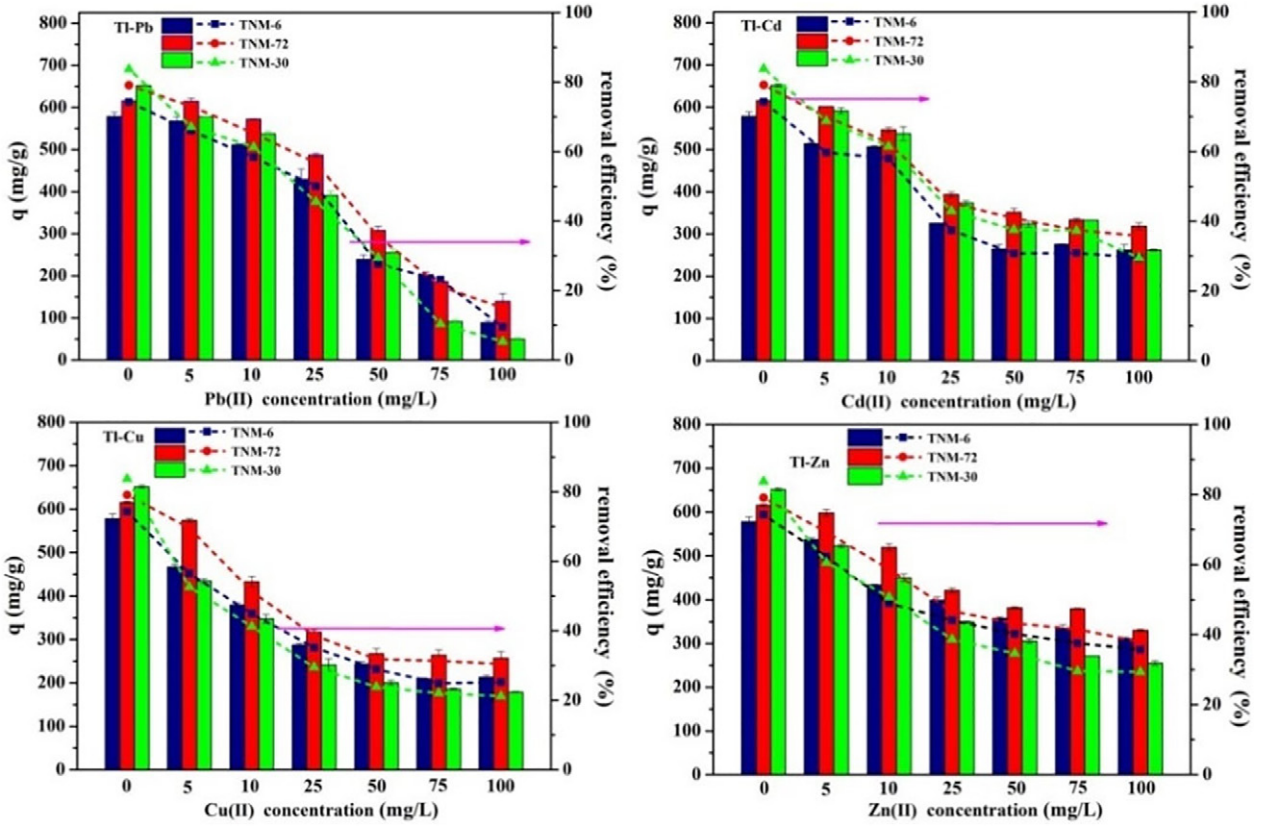

Fig. 5. Effects of coexisting Pb(II), Cu(II), Cd(II), and Zn(II) on Tl(I) adsorption by TNM-6, TNM-72, and TNM-30 (original solution pH, adsorbent dosage 0.25 g/L, Tl(I) concentration 200 mg/L, 25 °C).

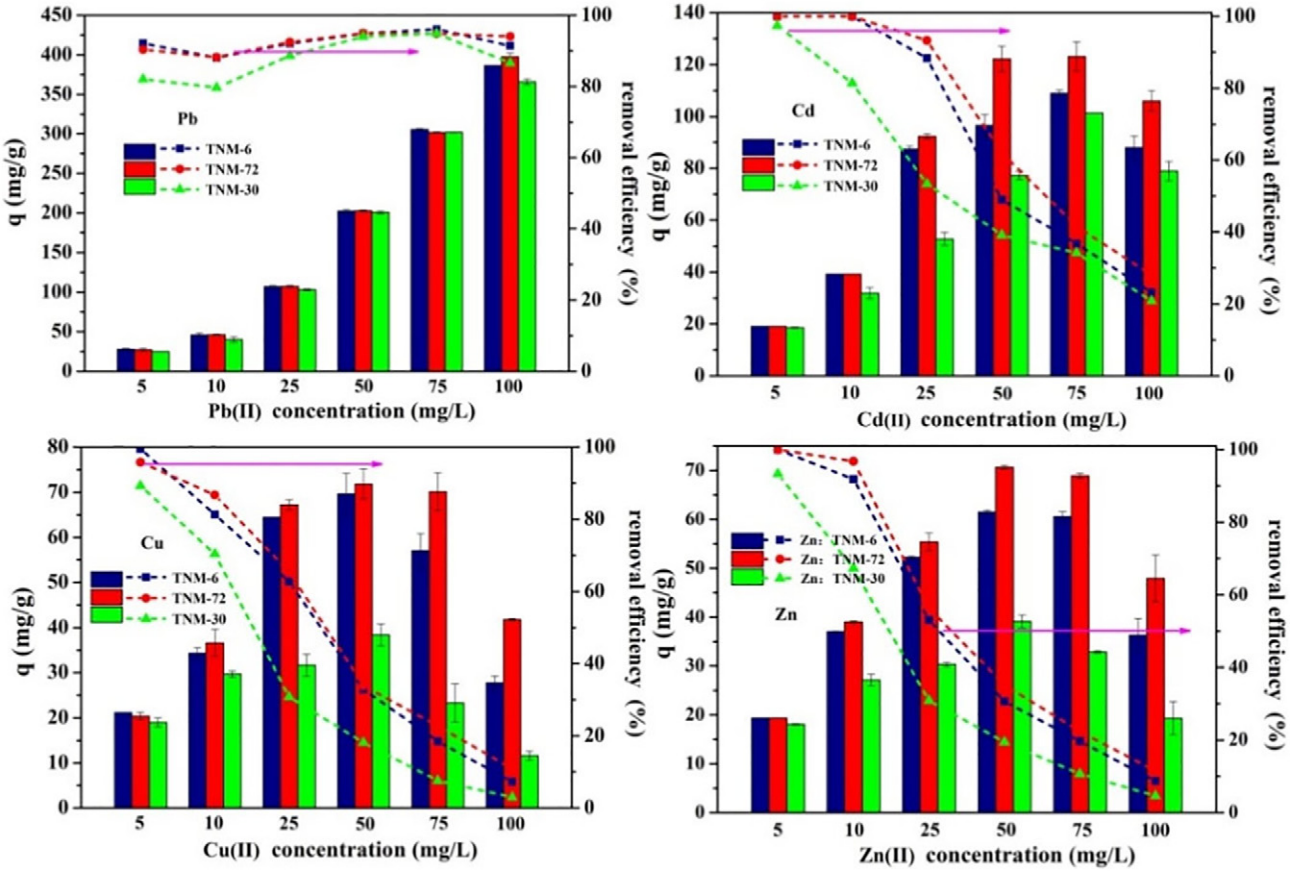

Fig. 6. Effects of Tl(I) on coexisting Pb(II), Cu(II), Cd(II), and Zn(II) adsorption by TNM-6, TNM-72, and TNM-30 (original solution pH, adsorbent dosage 0.25 g/L, Tl(I) concentration 200 mg/L, 25 °C).

ionic radii of the cations, the presence of Ca^{2+} exerted a stronger inhibition to the complexation interaction between Tl(I) and TNMs rather than ion exchange reaction with Na^{+}.

Ion adsorption through the cation exchange and/or outer-sphere complexation is driven by electrostatic forces and is sensitive to ionic strength variations, then the adsorption capacity will decrease with increasing ionic strength; while adsorption by forming inner-sphere complexes is less sensitive to changes in the ionic strength, thus the uptake percentage will increase or keep constant with increasing ionic strength (Zhang et al., 2018). According to this rule, Tl(I) adsorption on the three TNMs is mainly attributed to the formation of inner-sphere complexes, and the simultaneous formation of outer-sphere complexes plays a minor role. Thus, the underlying removal mechanisms of TNMs with different morphologies for Tl(I) might be consistent.

3.2.4. Selectivity of Tl(I) adsorption on TNMs

Considering the effects of coexisting heavy metals, competitive adsorption experiments among Tl(I) and Pb(II), Cu(II), Cd(II), Zn(II) were performed for four binary systems and one quinary system. The adsorption capacity (removal efficiency) of Tl(I) on TNM-6, TNM-72, and TNM-30 (Fig. 5) decreased as the concentration of the coexisting heavy metal ion increased in each binary system, indicating that all four heavy metals suppressed the adsorption of Tl(I) on TNMs to some extent, following the sequence of Pb(II) > Cu(II) > Cd(II) > Zn(II). Overall, there was insignificant difference in the anti-interference ability to coexisting heavy metal ions for the tubular and wire-like TNMs. As depicted in Fig. 6, for Cu(II), Cd(II), and Zn(II), the adsorption capacity firstly increased and then decreased as the initial concentration increased. The removal efficiency also sharply decreased from approximately 100%. In contrast, the adsorption capacity of Pb(II) kept increasing and its removal efficiency was always over 90%. The adsorption capacities of coexisting heavy metals on wire-like TNMs were lower than those on tubular TNMs, indicating the relatively higher selectivity of wire-like TNMs.

To determine the reasons for the abovementioned phenomena, the separation factors α_M^{Tl} (M = Pb, Cu, Cd or Zn) for all binary systems were introduced and calculated, as shown in Fig. 7. When α_M^{Tl} was >1, Tl(I) was preferentially adsorbed on TNMs in the binary system. In our study, the α_{Pb}^{Tl} values of TNMs were invariably smaller than 1 and gradually decreased with an increasing initial Pb(II) concentration,

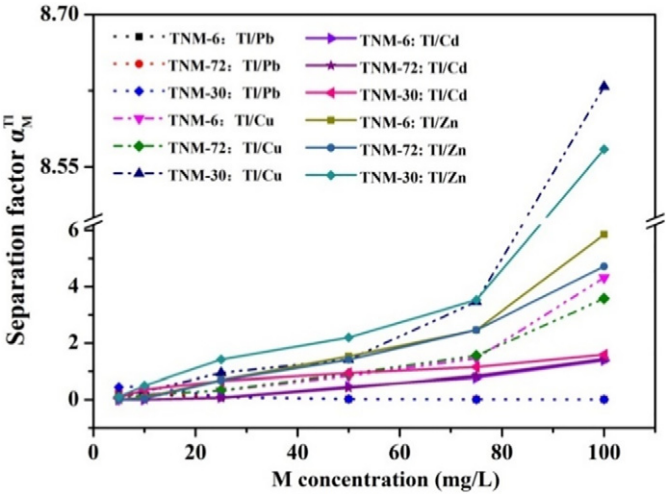

Fig. 7. Separation factors α_M^{Tl} (M = Pb, Cu, Cd or Zn) of Tl(I) on TNM-6, TNM-72, and TNM-30 in binary systems.

indicating that TNMs had a stronger preference for Pb(II) than for Tl(I). However, the α_{Cd}^{Tl}, α_{Cu}^{Tl} and α_{Zn}^{Tl} values remarkably increased with increasing Cu, Cd or Zn concentrations and were >1 at high concentrations. This result indicated that Tl(I) was preferentially adsorbed by TNMs in these binary systems. The order of $\alpha_{Zn}^{Tl} > \alpha_{Cu}^{Tl} > \alpha_{Cd}^{Tl}$ indicated the affinity order of Cd(II) > Cu(II) > Zn(II) to TNMs and the selectivity order of wire-like TNM-30 > tubular TNM-6/TNM-72. These might be dependent on the physicochemical properties of heavy metals such as ionic radius, hydration energy, hydrated radius, and electronegativity. In the quinary system (Fig. S5), the adsorption capacity of Tl (I) significantly decreased while that of Pb(II) steadily increased, and the adsorption amounts of Cd(II), Cu(II), and Zn(II) only slightly decreased. These properties of TNMs are conducive for practical applications in removing heavy metal ions from wastewater.

3.3. Adsorption mechanism

The mapping images and EDS spectra (Fig. 8 and Fig. S6) of the three TNMs before and after Tl(I) adsorption confirmed that ion exchange between Na^+ and Tl^+ was an important driving force in Tl(I) adsorption, due to the disappearance of Na accompanied by the emergence of Tl. The survey XPS results (Fig. S7) revealed that the Na 1s characteristic peak was significantly weakened after Tl(I) adsorption, whereas the Tl 4f characteristic peak appeared. This result was in accordance with the EDS analyses.

The spectra (Fig. 9) of tubular and wire-like TNMs had two peaks at approximately 464 eV and 458 eV, corresponding to Ti $2p_{1/2}$ and Ti $2p_{3/2}$, respectively. After Tl(I) adsorption, the Ti 2p characteristic peaks of TNM-30 insignificantly shifted, confirming that Ti(IV) did not participate in the Tl(I) adsorption reaction (Yin et al., 2017), while TNM-6 and TNM-72 had the opposite result. In the high-resolution O 1s spectra, the peaks at approximately 530.10 eV and 529.50 eV corresponded to crystal lattice oxygen in [TiO_6] octahedrons and Ti-O in $Na_3Ti_nO_{2n+1}$, and the shoulder peak at 531.40 eV was assigned to Ti–OH/Na (Liu et al., 2013; Liu et al., 2016). After Tl(I) adsorption, these peaks were almost consistent with the original ones, since the ion-exchange reaction did not alter the chemical composition of O; whereas the shoulder peaks of tubular.

TNMs appeared, due to the formation of Ti–O–Tl caused by the complexation. These results indicated that Na^+/H^+ mainly existed in the interlayers, and ion exchange occurred in the interlayers without affecting the basic skeleton [TiO_6] of TNMs.

Additionally, the Tl 4f energy spectra (Fig. 10a) of TNMs consistently presented four symmetrical peaks with a spin-orbital splitting of approximately 4.4 eV, corresponding to Tl $4f_{7/2}$ and Tl $4f_{5/2}$ (Deng et al., 2016). The Tl$4f_{2/7}$ peaks at approximately 118.55 eV and 119.10 eV are characteristic of Tl_2O and Tl(I), respectively. These results implied that Tl(I) was absorbed on the surface of TNMs in its original valence state and partly transformed into Tl_2O microprecipitation, which deposited on the adsorbent surface (Fig. S8). This could be indirectly proved

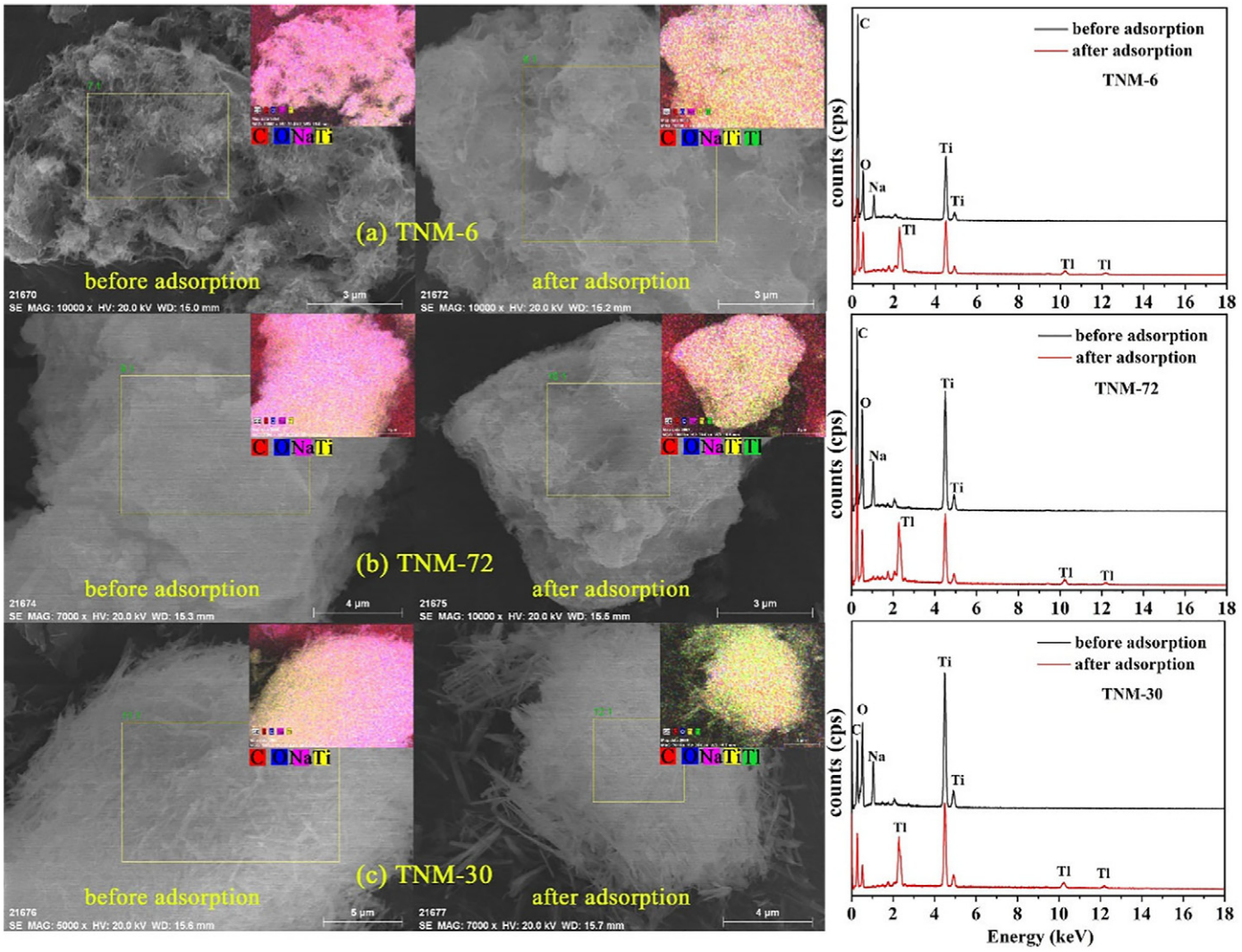

Fig. 8. SEM and EDS-mapping images of (a) TNM-6, (b) TNM-72 and (c) TNM-30 before and after Tl(I) adsorption.

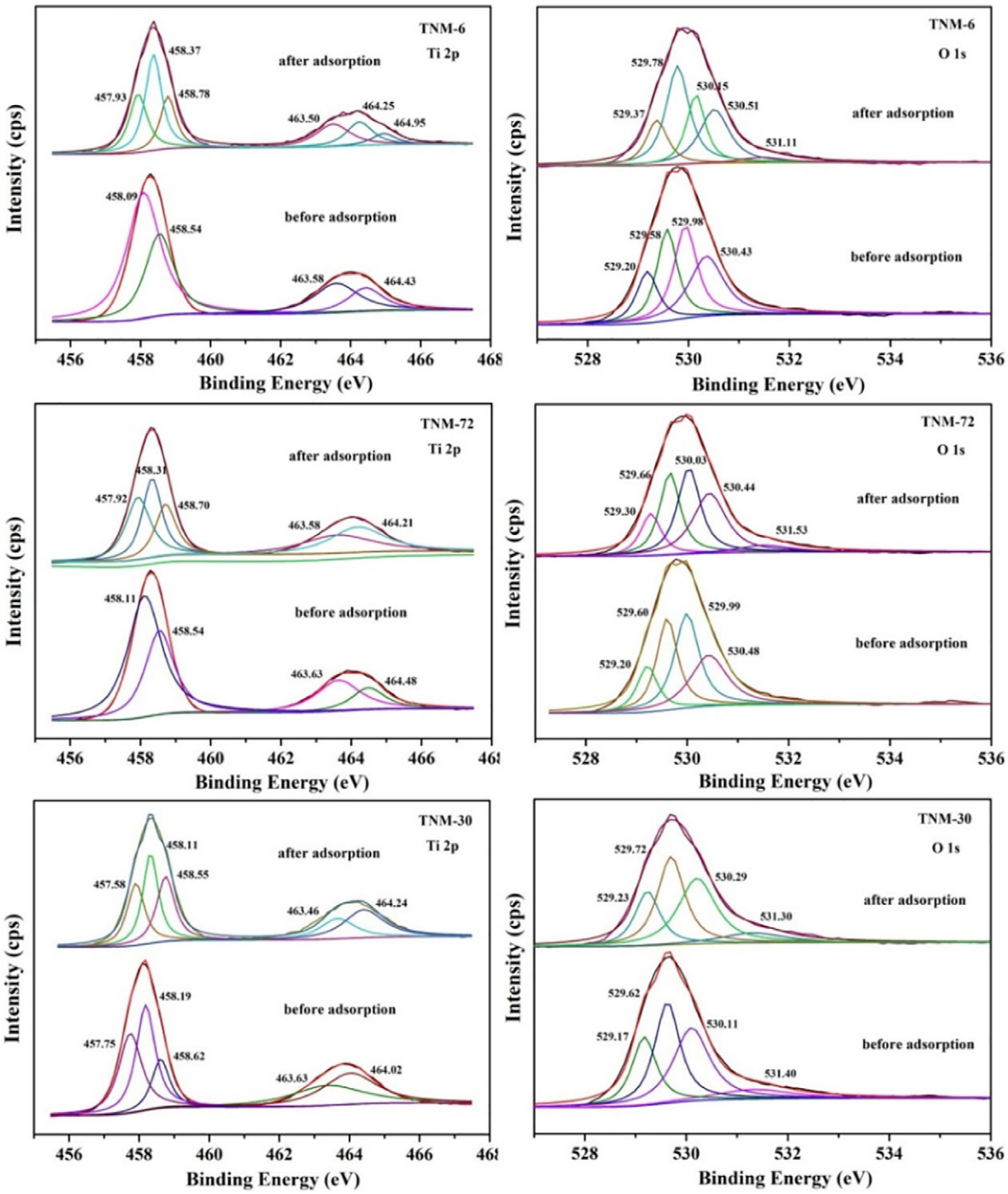

Fig. 9. XPS high-resolution spectra of Ti 2p and O 1s of TNM-6, TNM-72, and TNM-30 before and after Tl(I) adsorption.

by the changes of specific surface areas of TNM-6, TNM-72, and TNM-30 before and after Tl(I) adsorption, which markedly decreased from 174.85 to 87.72, 203.37 to 121.58 and 38.52 to 11.36 m^2/g, respectively.

As depicted in Fig. 10b, the broad peak at approximately 3430 cm^{-1} and the sharp peak at 1634 cm^{-1} were significantly weakened after Tl (I) adsorption. This was due to the dehydration process that the complexation of Tl(I) with the surface sites of TNMs occurred. Due to the replacement of H^+ in –OH and the ion exchange of Tl^+ with Na^+ in -ONa group, the peak at 3200 cm^{-1} completely disappeared while a new peak at 1383 cm^{-1} appeared, and the peaks around 905 cm^{-1} also shifted to 918 cm^{-1}. The new small peaks that appeared at 1159 and 1281 cm^{-1} were associated with inner-sphere complexation on the tubular TNMs (Li et al., 2017b), while the new peaks at 997 and 870 cm^{-1} indicated the formation of Ti–O–Tl on the surface of wire-like TNM-30 due to the disappearance of the peaks at 3200 and 910 cm^{-1}. This might imply that tubular TNMs and wire-like TNMs had different adsorption configurations. Moreover, the peaks in the range of 760–660 cm^{-1} that emerged after adsorption might be due to the microprecipitation of Tl(I) on the TNMs surface.

XRD characterization (Fig. 11) was used to further identify the potential binding modes of Tl(I) on TNMs. After the adsorption of Tl(I), the diffraction peak at $2\theta \approx 10°$ of the three TNMs completely

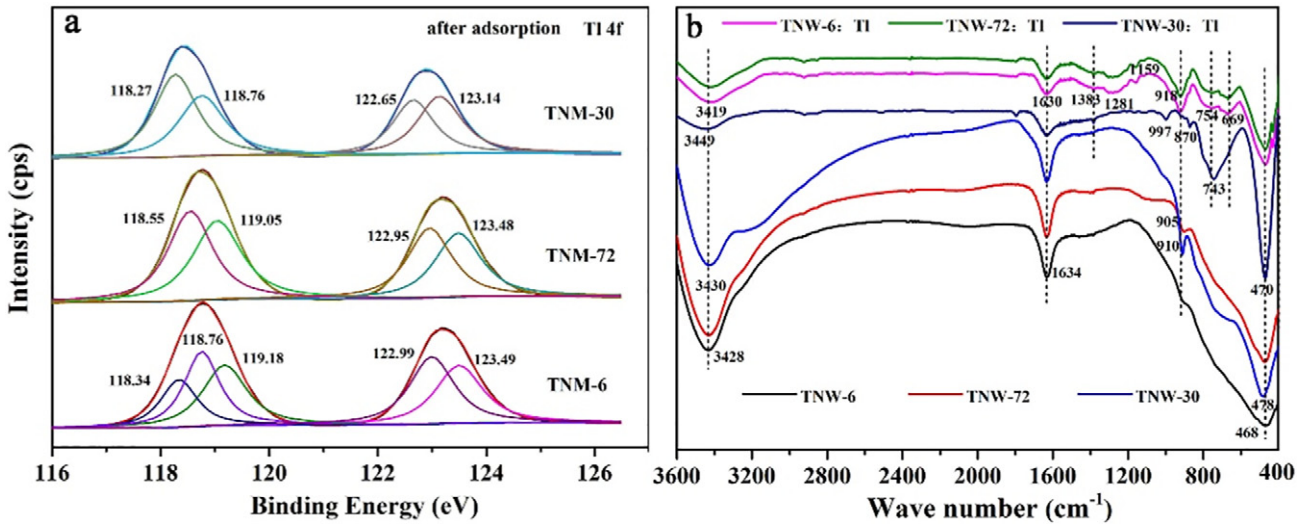

Fig. 10. (a) XPS high-resolution Tl 4f spectra and (b) FTIR spectra of TNM-6, TNM-72, and TNM-30 before and after Tl(I) adsorption.

disappeared. This was due to the strong ion exchange between Tl(I) and Na^+/H^+ in the interlayer of TNMs, which resulted in a reduction in the basal spacing, and also because the adsorbed Tl(I) caused disorder or even the breakage of the basic layered structure (Liu et al., 2014b; Yin et al., 2017). Furthermore, several other diffraction peaks were remarkably weakened or absent after Tl(I) adsorption, which were attributed to the effective replacement of Ti–O–Na by Ti–O–Tl and their participation in the adsorption reaction. The strong interaction between Tl (I) ions and negatively charged layers led to the significant decrease in (002) and increase in (003) diffraction intensities. The emergence of new peak at 32° assigned to Tl_2O (JCPDS card no. 28-1320) indicated the formation of Tl(I)-microprecipitation, which was consistent with the results of XPS and FTIR analyses.

According to the aforementioned analyses, there were insignificant differences in Tl(I) adsorption capacity and adsorption behaviors between tubular and wire-like TNMs, although there were some differences in the structures of three TNMs caused by the different synthesis conditions. Due to the similar types of functional groups on the three TNMs, the route of Tl(I) removal by tubular and wire-like TNMs is potentially consistent, except for the slight differences in adsorption configurations. Overall, the mechanism can be reasonably summarized as follows: first, Tl(I) ions moved to the surface of TNMs from the solution, driving by the electrostatic attraction; and then occurred the ion exchange reaction between Tl(I) and Na^+/H^+, followed the surface complexation through the dehydration process; whereafter, the formed complexes acted as nucleation sites for the further Tl (I) binding; eventually, they partly transformed into the microprecipitation and deposited on the surface of TNMs.

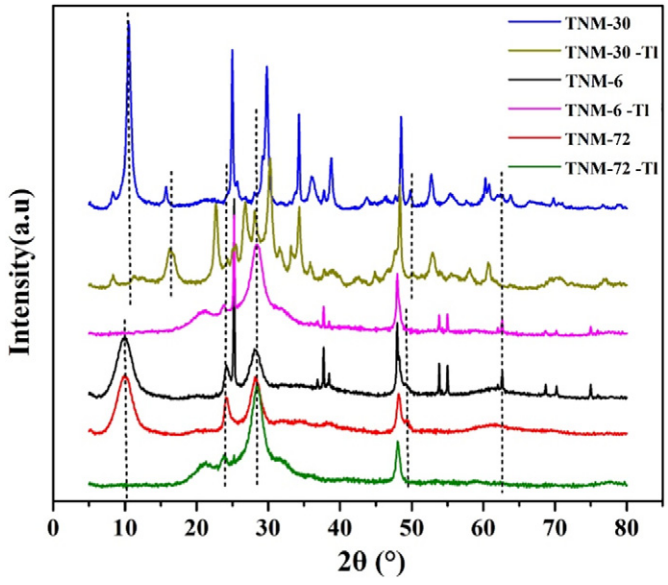

Fig. 11. XRD patterns of TNM-6, TNM-72, and TNM-30 before and after Tl(I) adsorption.

3.4. Potential applications of TNMs for removing metal(loid)s from natural water

Excellent adsorption capacity and regenerability are two important parameters used to evaluate the application feasibility of an adsorbent. For the as-prepared TNMs, the former had been confirmed, and the desorption experiments (data not shown) also indicated that Tl(I) could be readily eluted from TNMs by 0.1 M HNO_3 with desorption efficiencies over 90%. After regeneration with dilute NaOH solution and washing with water, the Tl(I) re-adsorption capacities of nanotubular and nanowire-like TNMs were approximately 85% and 80% of the corresponding original Tl(I) removal ability, respectively, which was higher than those regenerated by water. And the adsorption capacities of Tl (I) on as-prepared nanotubular and nanowire-like TNMs after the third adsorption-desorption cycle were maintained at the similar level as the former cycles. Furthermore, the specific surface areas of regenerated TNM-6 (161.39 m^2/g), TNM-72 (185.33 m^2/g), and TNM-30 (29.04 m^2/g) were slightly smaller than those of the original TNMs. The results indicated that the as-prepared TNMs can serve as a promising candidate for Tl(I) removal from water.

The Pearl River water samples spiked with different Tl (I) concentrations were used to assess the application potential of the as-prepared TNMs for removing metal(loid) ions from actual water samples. The pH value and turbidity of the water were 6.8–6.9 and 9.71 NTU, respectively. The residual concentrations of metal(loid) ions are summarized in Table 1. Tl(I) at initial concentrations of 141.45, 5512.26, and 27,384.13 μg/L was effectively removed by 0.25 g/L TNM-6, TNM-72, and TNM-30 with removal efficiencies over 98%; the concentrations of As, Cu, Cd, Pb, Ni, Zn, and Fe also decreased. These results indicated that the as-prepared TNMs can feasibly be used for the removal of trace and macro levels of metal(loid) ions from natural water, especially for Tl(I), which contributes to the security of water. Furthermore, the Na^+ concentration after adsorption by TNMs significantly increased, which further confirmed that ion exchange was one of the adsorption mechanisms.

Table 1
Metal(loid) ion concentrations of the spiked Pearl River waters before and after adsorption by TNMs.

Metals		Tl	As	Cu	Cd	Pb	Ni	Zn	Fe	Ba	Na	K
	c_0 (μg/L)	141.45	5.89	1.25	0.05	0.05	2.85	2.70	9.12	28.76	11,989	4378
TNM-6	c_e (μg/L)	3.21	2.46	0.60	0.01	0.02	1.20	1.52	4.17	0.14	29,697	3856
TNM-72		1.24	2.51	0.65	0.01	0.02	1.06	1.26	3.62	0.19	27,296	3528
TNM-30		1.54	3.77	0.73	0.00	0.03	2.38	1.71	5.06	0.33	26,841	3740
	c_0 (μg/L)	5512.26	5.38	1.23	0.06	0.05	2.84	2.97	8.79	29.57	12,108	4392
TNM-6	c_e (μg/L)	22.78	2.77	0.85	0.00	0.03	1.21	2.81	4.44	0.24	26,623	3891
TNM-72		14.12	2.48	0.85	0.01	0.02	1.25	2.05	3.71	0.25	27,220	3615
TNM-30		17.34	3.46	0.81	0.00	0.01	2.37	1.84	5.41	0.39	26,702	3817
	c_0 (μg/L)	27,384.13	5.48	1.39	0.05	0.04	2.93	2.72	8.59	28.89	11,767	4357
TNM-6	c_e (μg/L)	361.89	2.87	0.74	0.00	0.02	1.12	1.22	4.59	0.46	25,591	4300
TNM-72		98.80	2.47	0.72	0.00	0.03	1.09	1.21	4.40	0.45	22,271	3970
TNM-30		166.73	3.71	0.73	0.00	0.02	2.36	0.98	6.16	1.31	27,455	4183

4. Conclusions

In this study, we observed that titanate nanomaterials (TNMs) prepared under different synthesis conditions possessed different structural characteristics. The morphology of TNMs was significantly influenced by the temperature, due to the change of surface free energy. The tubular TNMs prepared at 130 °C and wire-like TNMs prepared at 180 °C were similar in the elementary composition and types of adsorption sites but different in the content and location of functional groups. Experimental results indicated that the tubular and wire-like TNMs both owned excellent Tl(I) removal efficiency over wide pH and temperature ranges; and the inhibition effects of heavy metals on Tl (I) removal and the adsorption preference of TNMs all followed the order of Pb(II) > Cu(II) > Cd(II) > Zn(II) and Pb(II) > Tl(I) > Cu(II) > Cd (II) > Zn(II), respectively. Tl(I) adsorption performances of tubular and wire-like TNMs were not mainly dependent on the morphology and crystal structure of TNMs. Tl(I) ions were effectively removed by TNMs under the action of electrostatic attraction, ion exchange, surface complexation, and microprecipitation. The regeneration tests indicated TNMs can be used as the promising candidate for Tl(I) removal in practical applications.

Our study directly demonstrated that the morphology (tubular and wire-like) of TNMs exhibited an unremarkable influence on the Tl (I) removal, and that the adsorption mechanisms were similar but the adsorption configuration had a slight difference. However, the special adsorption configurations and the changes in molecular and electronic structures as well as special energies upon adsorption, which are the driving forces underlining the Tl surface chemistry, are not fully understood. This fundamental knowledge about Tl chemistry at the TNMs-water interface is significantly important to grasp the transport and fate of Tl in the environment, which will contribute to the development of appropriate remediation and management strategies for Tl-contaminated waters and soils.

CRediT authorship contribution statement

Nana Wang: Conceptualization, Data curation, Writing - original draft. **Zebin Su:** Conceptualization, Methodology, Software, Validation. **Nairui Deng:** Formal analysis, Investigation. **Yuyin Qiu:** Formal analysis, Investigation. **Liang Ma:** Resources. **Jianqiao Wang:** Visualization. **Yuxiao Chen:** Supervision. **Kaimei Hu:** Data curation, Software. **Chujie Huang:** Validation, Methodology. **Tangfu Xiao:** Writing - review & editing.

Declaration of competing interest

The authors declare that they have no known competing financial interests or personal relationships that could have appeared to influence the work reported in this paper.

Acknowledgments

This work was funded by the National Natural Science Foundation of China (41830753; 41673138; 41907317; U1612442).

Appendix A. Supplementary data

Kinetics and isotherm models, SEM images, effect of the pH, Zeta potential, adsorption capacities of coexisting heavy metal ions, EDS-mapping images and XPS spectra after adsorption. Supplementary data to this article can be found online at https://doi.org/10.1016/j.scitotenv.2020.137090.

References

Belzile, N., Chen, Y.-W., 2017. Thallium in the environment: a critical review focused on natural waters, soils, sediments and airborne particles. Appl. Geochem. 84, 218–243. https://doi.org/10.1016/j.apgeochem.2017.06.013.

Carolin, C.F., Kumar, P.S., Saravanan, A., Joshiba, G.J., Naushad, M., 2017. Efficient techniques for the removal of toxic heavy metals from aquatic environment: a review. J Environ Chem Eng 5 (3), 2782–2799. https://doi.org/10.1016/j.jece.2017.05.029.

Chen, M., Wu, P., Yu, L., Liu, S., Ruan, B., Hu, H., Zhu, N., Lin, Z., 2017. FeOOH-loaded MnO_2 nano-composite: an efficient emergency material for thallium pollution incident. J. Environ. Manag. 192, 31–38. https://doi.org/10.1016/j.jenvman.2017.01.038.

Deng, H., Zhang, Z., Xu, N., Chen, Y., Wu, H., Liu, T., Ye, H., 2016. Removal of Tl(I) ions from aqueous solution using Fe@Fe_2O_3 core-shell nanowires. Clean – Soil, Air, Water 44 (9), 1214–1224. https://doi.org/10.1002/clen.201500403.

Hassanien, M.M., Mortada, W.I., Kenawy, I.M., El-Daly, H., 2017. Solid phase extraction and preconcentration of trace gallium, indium, and thallium using new modified amino silica. Appl. Spectrosc. 71 (2), 288–299. https://doi.org/10.1177/0003702816654166.

Huangfu, X., Ma, C., Ma, J., He, Q., Yang, C., Jiang, J., Wang, Y., Wu, Z., 2017. Significantly improving trace thallium removal from surface waters during coagulation enhanced by nanosized manganese dioxide. Chemosphere 168, 264–271. 264-271. https://doi.org/10.1016/j.chemosphere.2016.10.054.

Jia, Y., Xiao, T., Zhou, G., Ning, Z., 2013. Thallium at the interface of soil and green cabbage (*Brassica oleracea* L. *var. capitata* L.): soil–plant transfer and influencing factors. Sci. Total Environ. 450–451, 140–147. https://doi.org/10.1016/j.scitotenv.2013.02.008.

Jia, Y., Xiao, T., Sun, J., Yang, F., Baveye, P.C., 2018. Microcolumn-based speciation analysis of thallium in soil and green cabbage. Sci. Total Environ. 630, 146–153. https://doi.org/10.1016/j.scitotenv.2018.02.147.

Kanazawa, Y., Itadani, A., Hashimoto, H., Uematsu, K., Toda, K., Sato, M., 2019. Room temperature adsorption of propene and propane on copper ions distributed in titanate nanotubes. Appl. Surf. Sci. 483, 642–651. https://doi.org/10.1016/j.apsusc.2019.03.328.

Krasnodębska-Ostręga, B., Sadowska, M., Ostrowska, S., 2012. Thallium speciation in plant tissues—Tl(III) found in *Sinapis alba* L. grown in soil polluted with tailing sediment containing thallium minerals. Talanta 93, 326–329. https://doi.org/10.1016/j.talanta.2012.02.042.

Law, S., Turner, A., 2011. Thallium in the hydrosphere of south west England. Environ. Pollut. 159 (12), 3484–3489. https://doi.org/10.1016/j.envpol.2011.08.029.

Lee, C.-K., Lin, K.-S., Wu, C.-F., Lyu, M.-D., Lo, C.-C., 2008. Effects of synthesis temperature on the microstructures and basic dyes adsorption of titanate nanotubes. J. Hazard. Mater. 150 (3), 494–503. https://doi.org/10.1016/j.jhazmat.2007.04.129.

Li, X., Liu, W., Ni, J., 2015. Short-cut synthesis of tri-titanate nanotubes using nano-anatase: mechanism and application as an excellent adsorbent. Micropor. Mesopor Mater. 213, 40–47. https://doi.org/10.1016/j.micromeso.2015.04.018.

Li, S., Xiao, T., Zheng, B., 2012. Medical geology of arsenic, selenium and thallium in China. Sci. Total Environ. 421–422, 31–40. https://doi.org/10.1016/j.scitotenv.2011.02.040.

Li, H., Chen, Y., Long, J., Jiang, D., Liu, J., Li, S., Qi, J., Zhang, P., Wang, J., Gong, J., Wu, Q., Chen, D., 2017a. Simultaneous removal of thallium and chloride from a highly saline industrial wastewater using modified anion exchange resins. J. Hazard. Mater. 333, 179–185. https://doi.org/10.1016/j.jhazmat.2017.03.020.

Li, H., Chen, Y., Long, J., Li, X., Jiang, D., Zhang, P., Qi, J., Huang, X., Liu, J., Xu, R., Gong, J., 2017b. Removal of thallium from aqueous solutions using Fe-Mn binary oxides. J. Hazard. Mater. 338, 296–305. https://doi.org/10.1016/j.jhazmat.2017.05.033.

Liu, W., Wang, T., Borthwick, A.G.L., Wang, Y., Yin, X., Li, X., Ni, J., 2013. Adsorption of Pb^{2+}, Cd^{2+}, Cu^{2+} and Cr^{3+} onto titanate nanotubes: competition and effect of inorganic ions. Sci. Total Environ. 456–457, 171–180. https://doi.org/10.1016/j.scitotenv.2013.03.082.

Liu, W., Sun, W., Han, Y., Ahmad, M., Ni, J., 2014a. Adsorption of Cu(II) and Cd(II) on titanate nanomaterials synthesized via hydrothermal method under different NaOH concentrations: role of sodium content. Coll Surf A 452, 138–147. https://doi.org/10.1016/j.colsurfa.2014.03.093.

Liu, W., Zhang, P., Borthwick, A.G.L., Chen, H., Ni, J., 2014b. Adsorption mechanisms of thallium(I) and thallium(III) by titanate nanotubes: ion-exchange and co-precipitation. J Colloid Interf Sci 423, 67–75. https://doi.org/10.1016/j.jcis.2014.02.030.

Liu, W., Zhao, X., Wang, T., Zhao, D., Ni, J., 2016. Adsorption of U(VI) by multilayer titanate nanotubes: effects of inorganic cations, carbonate and natural organic matter. Chem. Eng. J. 286, 427–435. https://doi.org/10.1016/j.cej.2015.10.094.

Liu, Y., Wang, L., Wang, X., Huang, Z., Xu, C., Yang, T., Zhao, X., Qi, J., Ma, J., 2017. Highly efficient removal of trace thallium from contaminated source waters with ferrate: role of in situ formed ferric nanoparticle. Water Res. 124, 149–157. https://doi.org/10.1016/j.watres.2017.07.051.

Liu, J., Luo, X., Sun, Y., Tsang, D.C.W., Qi, J., Zhang, W., Li, N., Yin, M., Wang, J., Lippold, H., Chen, Y., Sheng, G., 2019. Thallium pollution in China and removal technologies for waters: a review. Environ. Int. 126, 771–790. https://doi.org/10.1016/j.envint.2019.01.076.

Madejón, P., Murillo, J.M., Marañón, T., Lepp, N.W., 2007. Factors affecting accumulation of thallium and other trace elements in two wild Brassicaceae spontaneously growing on soils contaminated by tailings dam waste. Chemosphere 67 (1), 20–28. https://doi.org/10.1016/j.chemosphere.2006.10.008.

Rodríguez-Mercado, J.J., Altamirano-Lozano, M.A., 2013. Genetic toxicology of thallium: a review. Drug and Chem Toxicol 36 (3), 369–383. https://doi.org/10.3109/01480545.2012.710633.

Sadowska, M., Biaduń, E., Krasnodębska-Ostręga, B., 2016. Stability of Tl(III) in the context of speciation analysis of thallium in plants. Chemosphere 144, 1216–1223. https://doi.org/10.1016/j.chemosphere.2015.09.079.

Simović, B., Dapčević, A., Zdravković, J., Tasić, N., Kovač, S., Krstić, J., Branković, G., 2019. From titania to titanates: phase and morphological transition in less alkaline medium under mild conditions. J Alloy. Compd. 781, 810–819. https://doi.org/10.1016/j.jallcom.2018.12.039.

Sun, X., Li, Y., 2003. Synthesis and characterization of ion-exchangeable titanate nanotubes. Chem. Eur. J. 9 (10), 2229–2238. https://doi.org/10.1002/chem.200204394.

Tatsi, K., Turner, A., Handy, R.D., Shaw, B.J., 2015. The acute toxicity of thallium to freshwater organisms: implications for risk assessment. Sci. Total Environ. 536, 382–390. https://doi.org/10.1016/j.scitotenv.2015.06.069.

Thorne, A., Kruth, A., Tunstall, D., Irvine, J.T.S., Zhou, W., 2005. Formation, structure, and stability of titanate nanotubes and their proton conductivity. J. Phys. Chem. B 109 (12), 5439–5444. https://doi.org/10.1021/jp047113f.

Twining, B.S., Twiss, M.R., Fisher, N.S., 2003. Oxidation of thallium by freshwater plankton communities. Environ Sci Technol 37 (12), 2720–2726. https://doi.org/10.1021/es026145i.

Wang, N., Xu, X., Li, H., Zhai, J., Yuan, L., Zhang, K., Yu, H., 2016. Preparation and application of a xanthate-modified thiourea chitosan sponge for the removal of Pb(II) from aqueous solutions. Ind. Eng. Chem. Res. 55 (17), 4960–4968. https://doi.org/10.1021/acs.iecr.6b00694.

Wu, D., Liu, J., Zhao, X., Li, A., Chen, Y., Ming, N., 2006. Sequence of events for the formation of titanate nanotubes, nanofibers, nanowires, and nanobelts. Chem. Mater. 18 (2), 547–553. https://doi.org/10.1021/cm0519075.

Xiao, T., Boyle, D., Guha, J., Rouleau, A., Hong, Y., Zheng, B., 2003. Groundwater-related thallium transfer processes and their impacts on the ecosystem: southwest Guizhou Province, China. Appl. Geochem. 18 (5), 675–691. https://doi.org/10.1016/S0883-2927(02)00154-3.

Xiao, T., Guha, J., Boyle, D., Liu, C.-Q., Zheng, B., Wilson, G.C., Rouleau, A., Chen, J., 2004. Naturally occurring thallium: a hidden geoenvironmental health hazard? Environ. Int. 30 (4), 501–507. https://doi.org/10.1016/j.envint.2003.10.004.

Xiao, T., Guha, J., Liu, C.-Q., Zheng, B., Wilson, G., Ning, Z., He, L., 2007. Potential health risk in areas of high natural concentrations of thallium and importance of urine screening. Appl. Geochem. 22 (5), 919–929. https://doi.org/10.1016/j.apgeochem.2007.02.008.

Xiao, T., Yang, F., Li, S., Zheng, B., Ning, Z., 2012. Thallium pollution in China: a geo-environmental perspective. Sci. Total Environ. 421–422, 51–58. https://doi.org/10.1016/j.scitotenv.2011.04.008.

Xu, H., Luo, Y., Wang, P., Zhu, J., Yang, Z., Liu, Z., 2019. Removal of thallium in water/wastewater: a review. Water Res. 165, 114981. https://doi.org/10.1016/j.watres.2019.114981.

Yin, L., Wang, P., Wen, T., Yu, S., Wang, X., Hayat, T., Alsaedi, A., Wang, X., 2017. Synthesis of layered titanate nanowires at low temperature and their application in efficient removal of U(VI). Environ. Pollut. 226 (Supplement C), 125–134. https://doi.org/10.1016/j.envpol.2017.03.078.

Zhang, G., Fan, F., Li, X., Qi, J., Chen, Y., 2018. Superior adsorption of thallium(I) on titanium peroxide: performance and mechanism. Chem. Eng. J. 331, 471–479. https://doi.org/10.1016/j.cej.2017.08.053.